RAA 2021 Vol. **21** No. **7**, 165(8pp) doi: 10.1088/1674-4527/21/7/165
© 2021 National Astronomical Observatories, CAS and IOP Publishing Ltd.
http://www.raa-journal.org *http://iopscience.iop.org/raa*

Research in Astronomy and Astrophysics

Distortion mapping correction in the AIMS primary mirror testing by a computer-generated hologram

Ke-Wei E[1], Jian-Ke Zhao[1], Bo Wang[2], Dong-Guang Wang[3], Yu-Liang Shen[3], Xin Fu[1], Song-Bo Xu[1], Jing Li[1], Xun Xue[1], Ming Chang[1] and Yan Zhou[1]

[1] Xi'an Institute of Optics and Precision Mechanics, Chinese Academy of Sciences, Xi'an 710119, China; *ekewei@opt.ac.cn*

[2] Nanjing Astronomical Instruments, Chinese Academy of Sciences, Nanjing 210042, China

[3] National Astronomical Observatories, Chinese Academy of Sciences, Beijing 100101, China

Received 2020 November 10; accepted 2021 February 19

Abstract The National Solar Observatory is currently developing the Accurate Infrared Magnetic Field Measurements of the Sun (AIMS). The primary mirror of the AIMS solar telescope is an off-axis parabolic with a diameter of 1 m and with a large off-axis amount of 1 m. Due to the surface figure of the primary mirror under the used state is directly related to image quality of the whole system, a computer-generated hologram (CGH) is carried out to test the primary mirror, and the test results are used to polish the mirror to a higher surface accuracy. However, the fact that the distortion exists in the testing results leads to the failure of a further guide to deterministic optical processing. In this paper, a distortion correction method is proposed, which uses an orthogonal set of vector polynomials to mapping the coordinates of the mirror and the pixels of fringes, and then an interpolation method is adopted to obtain the corrected results. The testing accuracy by using CGH is also verified by an auto-collimate test experiment. According to the distorted corrected results, the root-mean-square of the surface figure is about 1/50λ (λ=632.8 nm) after polishing.

Key words: telescopes — techniques: interferometric — methods: astronomical instrumentation, methods and techniques

1 INTRODUCTION

The testing and manufacturing of the large aperture optical mirrors are one of the cutting-edge projects of current hard technology, which undoubtedly has an important application value for a series of applications such as space remote imaging and high energy laser system. Along with the increase of the aperture of mirrors, more requirements are put forward for optical testing. For example, AIMS, which is abbreviation of "an infrared system for the accurate measurement of solar magnetic field", is a national major scientific research project currently developed. The guiding optical system of AIMS is an off-axis Gregorian system, while the primary mirror is an off-axis parabolic mirror with a diameter of 1m and off-axis amount of 1 m (Jiang & Jiang 2020; Xun et al. 2020). The surface error of the primary mirror of AIMS will directly affect the imaging accuracy of 8–10 μm imaging system, BRUCKER spectrometer and other rear optical system. When the AIMS tracking the sun, the minimum angle between the optical axis of the primary mirror and horizontal plane is 14.036°, the wavefront of the guiding optical system in this condition need to reach 1/15λ RMS in order to satisfy the need of observation of solar magnitude, hence it is very critical to test and polish the mirror to a high accuracy in this condition.

A commonly used surface testing method to test such off-axis parabolic mirror is the auto-collimate test, which is realized by a focal plane interferometer and an auto-collimator flat of the same aperture as with the test mirror. However, the 1 m level diameter mirror is hard for fabrication and testing, moreover, when the head is tilted at 14.036° to measure the surface shape of the AIMS primary mirror, the surface shape accuracy of the reference mirror itself cannot be guaranteed, thereby influencing the test accuracy (Chen et al. 1992). Another method that can reduce the measurement error induced by the reference mirror surface error is the sub-aperture stitching test. Such a stitching test uses an optical flat smaller than the system aperture under test to obtain sub-aperture wavefront, and then synthesize a full aperture surface figure from these sub-aperture wavefronts with a set of mathematical techniques. The efficiency of this method is poor because it needs to be measured at multiple locations. During the stitching process, factors such as airflow disturbances and environmental temperature changes will have greater impact on the test, therefore, it is challenging to using this method to test the primary mirror especially in the polishing stage. On the other hand, one can make a second optical system that converts the wavefront produced by the primary mirror into either a spherical or plane wavefront, due to the primary mirror of the AIMS has a large deviation from the closet spherical surface, the null optics needs to compensate for a large aberration. If a null lens is used, it is necessary to strictly control the center thickness, spacing, curvature radius, and refractive index of each lens of the compensator, which is often expensive to produce accurately, therefore other methods need to be employed to calibrate the null lens system error.

Computer-generated holograms (CGHs) have advantages over null lens, including small volume, light weight and more design freedom. In principle, it can produce arbitrary reference wavefront for measuring the shape of the aspheric surface, therefore, CGHs are widely used in the testing aspheric optics (Wyant & Bennett 1972; Burge et al. 2006, 2008). In this paper, according to the requirements of the AIMS and the parameter of primary mirror, a CGH plate is designed and test equipment is built. Since the primary mirror have a large off-axis amount and the limitation of size of the CGH, a large nonlinear distortion exists in the test data, and the presence of that distortion makes it impossible to perform the polishing process and must be corrected. In this paper, a distortion correction method is proposed which is a combination of the orthogonal vector polynomials fitting and an interpolation scheme. The test results after correction are also verified using an auto-collimation test on the primary mirror in the two postures with the optical axis in the horizontal plane. And then, according to the CGH test results, the primary mirror was polished when the angle between the optical axis of the primary mirror and the horizontal plane was $14.036°$.

The paper is organized as follows. In Section 2, we described the process of CGH for a primary mirror in detail, the distortion correction method is given in Section 3. Experimental results of correcting the distorted surface figure, verification experiments using the auto-collimation test, and the polishing process are presented in Section 4. Finally, Section 5 contains our concluding remarks.

2 CGH FOR AIMS PRIMARY MIRROR

The 1100 mm diameter F/2 primary mirror of AIMS is an off-axis parabolic mirror, and its off-axis amounts is 1000 mm. The geometric drawing is shown in Figure 1. When the primary mirror is in a vertical state, the angle between its optical axis and the horizontal plane is $14.036°$.

The schematic diagram of the testing setup of the primary mirror using CGH is shown in Figure 2. As exhibited in Figure 2, the spherical wave emitted by the interferometer is focused on a point, and then passes through the CGH. The CGH performs the phase converter to transform the spherical wave to a specific wavefront that satisfies the condition that when it propagating to the surface of the primary mirror, the direction of the light is consistent with the normal direction of the primary mirror. To begin the design of the CGH using optical design software, one can do so using a reverse ray tracing strategy. Supposing the light beam emerges from a fictitious zero-index glass, and is refracted by the aspheric surface boundary, and then enters to the air, thereby the emitted beam is perpendicular to the surface of the primary mirror. An optimization process is performed to optimize the spatial position and phase distribution of the CGH, so that the residual aberration at the point source is the smallest (Li et al. 2013; Peng et al. 2015).

The relative position of the CGH relative to the point source and the primary mirror determines the phase distribution of the CGH. The mapping distortion, CGH processing level, and the required linear carrier frequency to separate the diffraction orders should be comprehensively considered to ensure that the designed CGH meets the requirements of the testing (Zhou & Burge 2007; Lindlein 2001). The designed distance from the point source to the CGH is 250 mm, and the distance from the CGH to the primary mirror is 3891.7 mm as shown in Figure 2.

The designed CGH is shown in Figure 3, which is a 6-inch in diameter quartz plate with a thickness of 6.4 mm. The oval shape area in Figure 3(a) is the main hologram, which is a phase type hologram used to measure the shape of the primary mirror. The ring-shaped area is an alignment hologram, which is an amplitude-type hologram used to align the relative position between the interferometer and the CGH. The four circular areas are mark holograms, which are phase holograms that used to realize the coarse align the primary mirror, CGH and interferometer. The setting-up process of the test setup and the sequence of the alignment will described later in the experimental section.

The physical picture of the CGH is shown in Figure 3(b), the minimum scribe line of the main hologram and alignment hologram is 2.4 μm and 3.6 μm respectively.

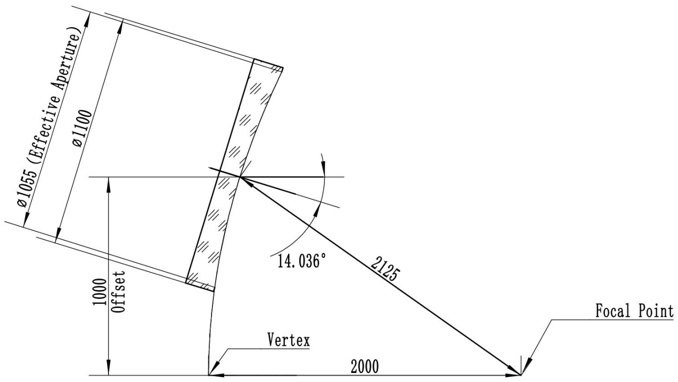

Fig. 1 Geometric drawing of the AIMS primary mirror.

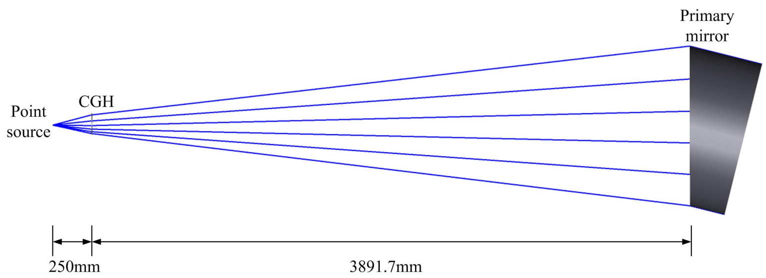

Fig. 2 Optical layout for testing the AIMS primary mirror with CGH.

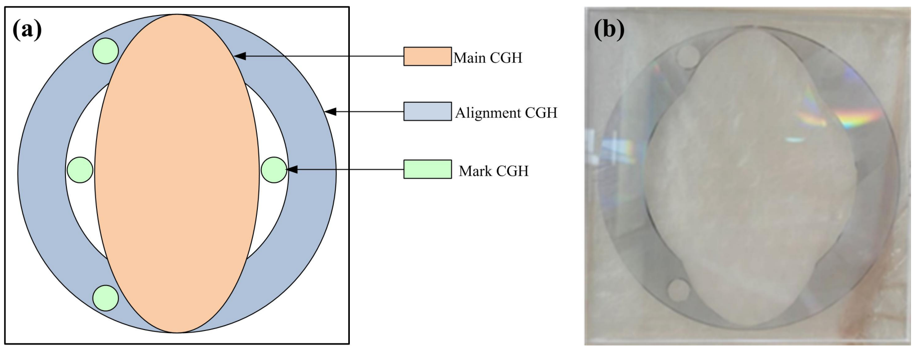

Fig. 3 Layout diagram of the designed CGH: (a) schematic diagram and (b) physical picture.

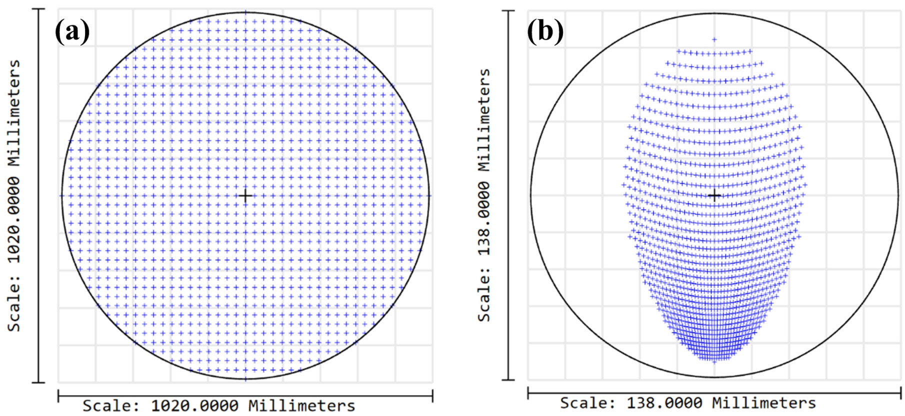

Fig. 4 Beam footprint: (a) at the primary mirror and (b) at CGH.

3 DISTORTION CORRECTION METHOD

Imperfect imaging through the CGH results in a non-linear mapping relationship between the surface coordinates of the mirror under test and the corresponding coordinates on the interferometer detector. The difference in the distance between the CGH and the mirror under test will introduce different distortions (Zeng et al. 2018). Figure 4 shows the footprints of the primary mirror surface and the CGH. It can be seen from the figure that there are serious nonlinear distortions in the test system.

The distortion presented here needs to be accurately corrected, the main reasons are: (a) During the test of the primary mirror, the coefficients of the low-order terms of the Zernike polynomial (such as defocus, astigmatism, coma, etc.) need to be adjusted as small as possible through aligning the optics in the test setup so that the test results accurately reflect the real surface shape of the primary mirror. When such distortion exists, the various aberration items will be coupled with each other. For example, when the tilt x aberration on the distorted wavefront is corrected and mapping to the regular coordinates, there is a larger astigmatism component, and when the coma term on the distorted area is transformed into an undistorted circular area, a larger spherical aberration component will appear. This is not conducive to the precise adjustment of the test system. (b) When polishing the primary mirror, the coordinate of the surface figure data needs to be accurately positioned, since the surface figure has a large non-linear distortion, high-precision polishing cannot be completed if the distortion correction is not performed (Zhao & Burge 2009).

Commonly used distortion correction methods generally assume that no distortion exists between the CGH and the interferometer detector. Therefore, after applying ray tracing according to the designed model, the coordinate correspondence between the measured mirror and the CGH can be calculated, and then the distortion can be corrected. However, there is deviations between the actual optical test system and the designed model, moreover, the imaging lens of the interferometer also has distortion, so that this method cannot meet the high-precision test requirements (Zhao & Burge 2009).

For solving the problems mentioned above, we have made fiducials with known coordinates on the primary mirror. After obtaining the corresponding centroid position of image of these fiducials, the following mapping relationship is established:

$$\boldsymbol{r}_{\text{distorted}} = M(\boldsymbol{r}_{\text{undistorted}})\,. \tag{1}$$

In Equation (1), M is a mapping function, which realizes the mapping from undistorted points to distorted points, where $\boldsymbol{r}_{\text{distorted}}$ is the set of the point coordinates in the distorted map with units of pixels and assumes the coordinates are ($x^{'}$,$y^{'}$), $\boldsymbol{r}_{\text{undistorted}}$ is the set of the point coordinates in the test mirror with the units of mm and assumes the coordinates are (x,y). The mapping relationship M can be obtained by fitting the known $\boldsymbol{r}_{\text{distorted}}$ and $\boldsymbol{r}_{\text{undistorted}}$ sets. An orthogonal vector Zernike polynomial set, namely S and T polynomials are used to obtain the mapping relationship M (Zhao & Burge 2007, 2008). Assuming that the S vector polynomial indices is S_ind=[4∼J] and the T vector polynomial indices is T_ind=[4∼L]. For a given S_j with corresponding indices j ∈ S_ind at an undistorted point p, its x and y components at this point can be defined as $S_{xp,j}$ and $S_{yp,j}$ respectively. Similarly, $T_{xp,j}$ and $T_{yp,j}$ represent the x and y components of T_j with corresponding indices j ∈ T_ind at point p. If the number of fiducials is n, then the mapping relationship can be given by the following formula:

$$\begin{bmatrix} x_1^{'} \\ \dots \\ x_n^{'} \\ y_1^{'} \\ \dots \\ y_n^{'} \end{bmatrix} = \begin{bmatrix} S_{x1,4} & \dots & S_{x1,i} & \dots & S_{x1,J} & T_{x1,4} & \dots & T_{x1,j} & \dots & T_{x1,L} \\ \dots & \dots & \dots & \dots & \dots & \dots & \dots & \dots & \dots & \dots \\ S_{xn,4} & \dots & S_{xn,i} & \dots & S_{xn,J} & T_{xn,4} & \dots & T_{xn,j} & \dots & T_{xn,L} \\ S_{y1,4} & \dots & S_{y1,i} & \dots & S_{y1,J} & T_{y1,4} & \dots & T_{y1,j} & \dots & T_{y1,L} \\ \dots & \dots & \dots & \dots & \dots & \dots & \dots & \dots & \dots & \dots \\ S_{yn,4} & \dots & S_{yn,i} & \dots & S_{yn,J} & T_{yn,4} & \dots & T_{yn,j} & \dots & T_{yn,L} \end{bmatrix} \cdot \begin{bmatrix} s_4 \\ \dots \\ s_J \\ t_4 \\ \dots \\ t_L \end{bmatrix}\,, \tag{2}$$

here $s_4 \sim s_J$, $t_4 \sim t_J$ are fitting coefficients, the mapping function $M(s_4 \cdots s_{13}, t_4 \cdots t_{13})$ can be calculated by using a least squares algorithm.

Once the M function is determined, the distortion pixel coordinates corresponding to each regular point can be obtained. Suppose the distorted pixel coordinates that mapped from the regular points is p, and the surface shape data at this point is represented by $W(p)$. The surface shape data of the four nearest points at p are known and assuming that it can be represented by W_{lu}, W_{ru}, W_{ld} and W_{rd} respectively. The distances from p to its closest upper

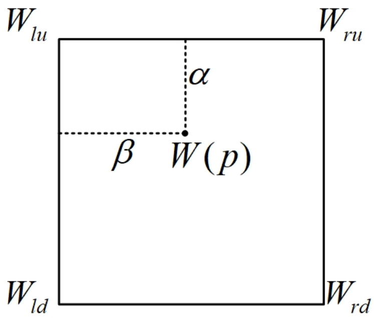

Fig. 5 Schematic diagram of the interpolation method.

left integer point in the row and column directions are α and β respectively, as shown in Figure 5. And then the $W(p)$ can be obtained by using the equation below:

$$W_p = (1-\alpha)\cdot(1-\beta)\cdot W_{lu} + \alpha\cdot(1-\beta)\cdot W_{ld} + (1-\alpha)\cdot\beta\cdot W_{ru} + \alpha\cdot\beta\cdot W_{rd}\,. \tag{3}$$

4 EXPERIMENT

4.1 Setup and System Alignment

The PhaseCam 6100 interferometer with an F-number of 2 produced by 4D company is used as the testing equipment, and the resolution of the detector is 2K×2K. The primary mirror is measured in a condition that the angle between the optical axis of the mirror and horizontal plane is $14.036°$. For convenience of description, the point on the mirror that is closest and farthest to the vertex of the parabolic parent mirror are represented as L and H respectively. The test mirror can be rotated around the x-axis, y-axis or z-axis by mechanical structures. On the other hand, the main parts of the test equipment, including the 4D interferometer and the CGH, are aligned together and installed on one table located on a six-axis adjustment mechanism. The measurement setup is shown in Figure 6.

The test setup is built according to Figure 2, and the sequence is as follows:

(a) Use the alignment hologram to adjust position and the orientation of the CGH and interferometer in such a way that the number of the fringes reflected by the hologram is minimum. After completing this alignment, the interferometer and the CGH are treated as a whole and the relative position cannot be changed throughout the testing process.

(b) Set the distance of the CGH between the primary mirror with accuracy better than 5 mm. Find the four markers position projected by the mark CGH and then adjust the orientation of the primary mirror or the position and orientation of the CGH and interferometer, so that the projected markers are at the edge of the primary mirror.

(c) Adjust the orientation of the CGH and interferometer as a whole such that the minimum light spot that reflected from the primary mirror under test and diffracted by CGH coincides with the focal point of the interferometer. After coarse alignment mentioned above, interference fringes can be observed on the interferometer detector. And then the six-dimensional adjustment mechanism is used again to fine-tune the overall position and orientation of the interferometer and the CGH, so that the astigmatism and coma terms in the surface shape data are the smallest. An interference fringe captured by the interferometer is shown in Figure 7.

4.2 Distortion Correction

It can be seen from Figure 7 that the interference fringe has obvious distortion. In order to realize the distortion correction, the mark points distribution as shown in Figure 8(a) are designed. The first point, around which the other 36 marker points are distributed on three circles, is set in the center of the mirror. The first circle includes six evenly distributed points and the radius is 167 mm. While the second and the third circle with a radius of 334 mm and 501 mm includes 12 and 18 evenly distributed points respectively. And then markers are marked on the primary mirror according to the coordinates of these points by using a coordinate measuring machine. In order to ensure that the size of the images of each fiducial is basically the same, three types of square fiducials with a side length of 1 cm, 1.5 cm and 2 cm are designed, and the number of these fiducials are 4, 11, and 22 respectively. These designed fiducials are pasted on the mirror to the corresponding points as shown in Figure 8(b). Figure 8(c) shows the images corresponding to the fiducials that can be clearly seen from the modulation of the interference fringe.

The center of gravity of the fiducial images are calculated and then its normalized coordinates can be obtained, which is denoted by red circles as in Figure 9(a). In addition, the blue crosses in Figure 9(a) represent normalized coordinates of regular points on the primary mirror. These coordinates can be used to generate a distortion vector represented by the blue arrow as shown in Figure 9(b). The distortion vectors are fitted using the first 2 to 13 terms of the S and T vector polynomials described earlier in Section 3, and the fitted result is plotted in Figure 9(b) and is denoted by red arrows. It is evident from Figure 9 that the tested distortion vectors coincide with the fitted results, and further analyzing the data indicates that the root mean square error of re-projection error is 0.003, which corresponds to 2.67 pixels and 1.59 mm in the image coordinates and mirror coordinates respectively. That accuracy is sufficient enough to polish the primary mirror under the current level of processing.

Table 1 The Number of Polishing and Its Corresponding RMS of Surface Error of Primary Mirror in Effective Aperture

Number of polishing	2	4	6	8	10	12
RMS of surface error (Units:λ)	0.0340	0.0308	0.0295	0.0262	0.0269	0.0198

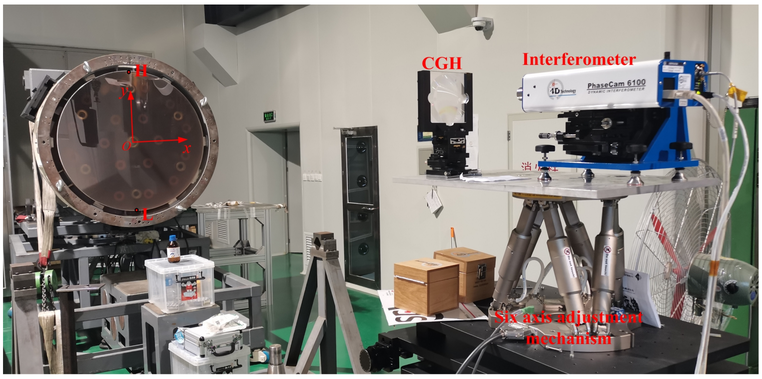

Fig. 6 Primary mirror testing setup.

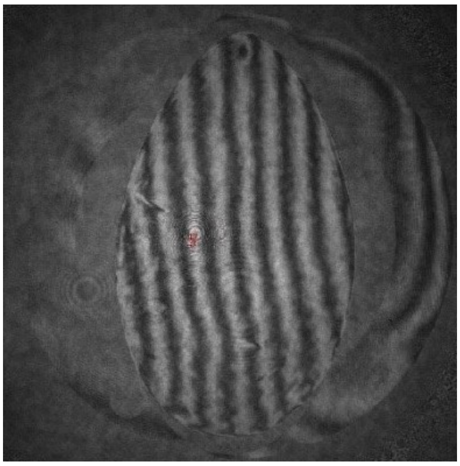

Fig. 7 Interference fringe.

The surface figure tested using the CGH is shown in Figure 10(a), the distortion corrected surface figure can be obtained by using the distortion correction method described in section 3 and is shown in Figure 10(b).

4.3 Verification Experiments

The testing accuracy of CGH needs to be evaluated before polishing the primary mirror to a higher accuracy. An auto-collimate testing scheme to verify the testing accuracy were designed as shown in Figure 11. The H, L point and the focal point of the interferometer in Figure 11 are in the horizontal plane (xoz). In the first verification experiment, the H is at the $-x$ direction as shown in Figure 11(a), while in the second verification experiment, H is at the $+x$ direction, which is shown in Figure 11(b).

Correspondingly, the CGH was also used to test the primary mirror in these two states, the comparison results are shown in Figure 12. Comparing the results of the CGH and the auto-collimate testing shown in Figures 12(a), (b), (c) and (d), it can be seen that similar features can be found in both test results, and the RMS of the surface error are very close. This verifies the accuracy of the CGH testing approach and the correctness of our distortion correction algorithm.

After completing the validation of the accuracy of the CGH testing approach and the distortion correction algorithm, the primary mirror is polished manually multiple times. The number of polishing and its corresponding RMS error of the primary mirror within effective aperture are listed in Table 1. Table 1 shows the RMS of surface error converges to about $1/50\lambda$ RMS after polishing 12 times. The final figure of the primary mirror within the effective aperture is shown in Figure 13. Comparing Figure 13 and Figure 10(b), the surface shape in Figure 13 is more uniform, and the three areas with large surface shape fluctuation (dark blue areas) in Figure 10(b) disappeared in Figure 13. Even though the polishing process can further improve the figure accuracy, the surface figure of the primary mirror in Figure 13 already meets the requirements of the AIMS.

5 CONCLUSIONS

The surface error of the AIMS primary mirror directly affects the imaging quality of a back-end optical system, which makes it critical to test the primary to high accuracy. In order to meet the requirements of usage of the AIMS primary mirror, a CGH for the primary is designed and a testing system is built in this paper. The nonlinear mapping relationship between the primary mirror and the fringe captured by the interferometer are first fitted using

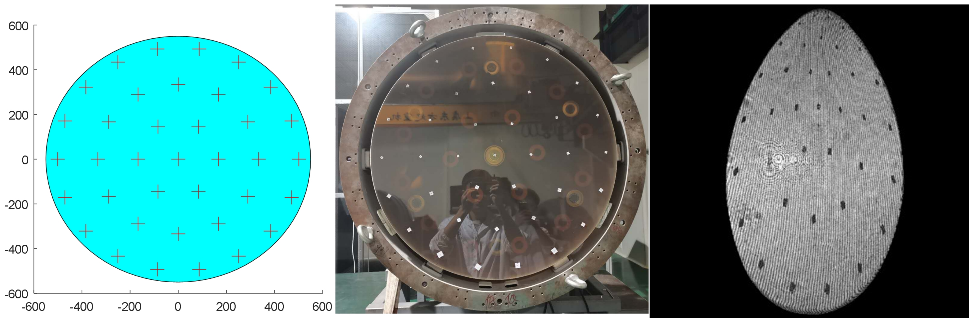

Fig. 8 Layout of fiducials and its image: (a) distribution of the markers, (b) primary mirror with 37 fiducials and (c) modulation of the interference.

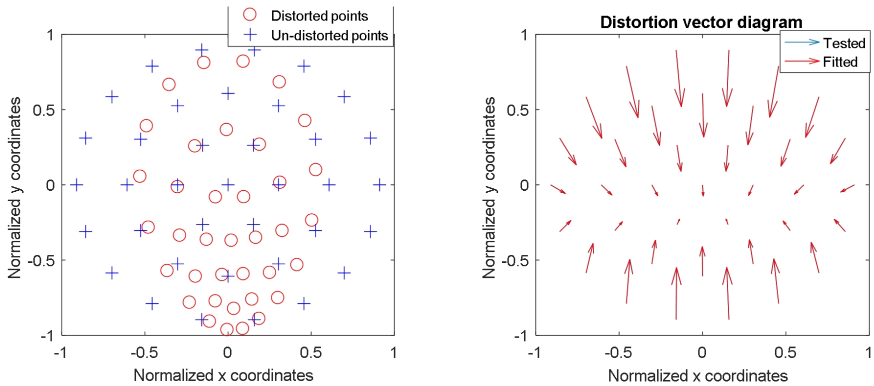

Fig. 9 Mapping the relationship between the coordinates of image of fiducials and the regular points on the mirror by using vector polynomials: (a) normalized coordinates of regular points and image of the fiducials and (b) the tested distortion vector diagram and its fitted results.

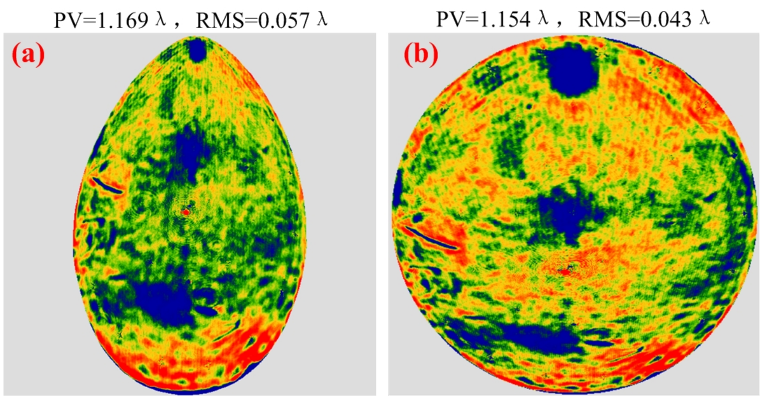

Fig. 10 Tested surface figure of the primary mirror: (a) distorted surface figure and (b) distortion corrected surface figure.

the orthogonal vector Zernike polynomials, and then an interpolation strategy was adopted to correct the distorted surface figure. To validate the testing approach discussed above, validation experiments are implemented. In our validation experiments, the primary mirror is placed in a state such that the axis is in the horizontal plane and the mirror is tested using both the CGH testing approach described in this paper and an auto-collimate testing method. The consistency of the results measured by these two methods verifies the correctness of the CGH testing approach used in this article. Finally, the primary mirror was polished manually according to the CGH testing results and the surface error reached $1/50\lambda$ RMS after polishing 12 times. The method presented in this paper can provide helpful references for testing large aperture optical mirror.

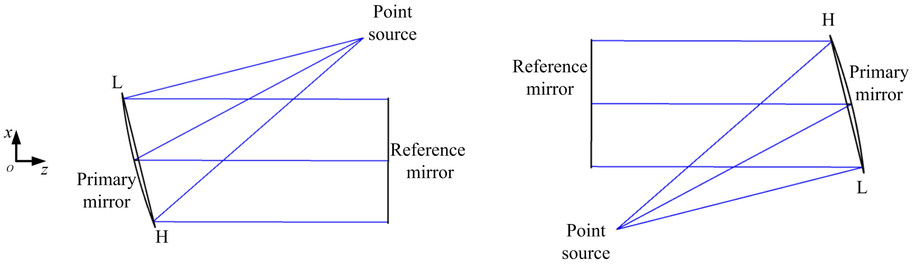

(a) (b)

Fig. 11 Primary mirror testing setup by using the auto-collimate test method: (a) H at - x direction and (b) H at + x direction.

Test method	Position	
	H point at -x direction	H point at x direction
Auto-collimate test	PV=0.526 λ ,RMS=0.043 λ 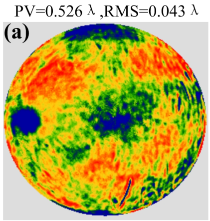	PV=0.474 λ ,RMS=0.038 λ 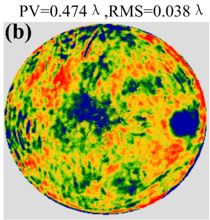
CGH test	PV=1.177 λ ,RMS=0.045 λ 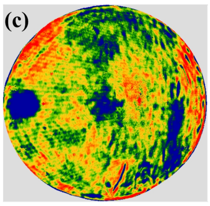	PV=0.100 λ ,RMS=0.045 λ 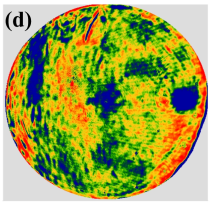

Fig. 12 Comparison of the testing results of the primary mirror: (a) auto-collimate test, H points at -x direction, (b) auto-collimate test, H points at +x direction, (c) CGH test, H points at -x direction and (d) CGH test, H points at +x direction.

PV=0.730 λ , RMS=0.020 λ

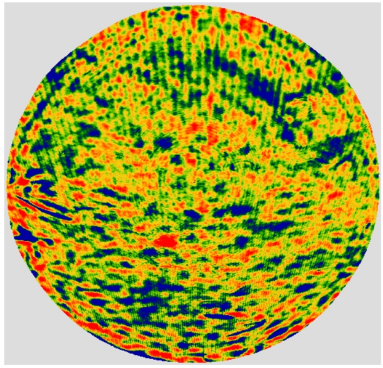

Fig. 13 Final surface figure of the primary mirror within effective aperture.

Acknowledgements This work was funded by the West Light Foundation of the Chinese Academy of Sciences (Grant No. XAB2017B13) and by the National Natural Science Foundation of China (Grant No. 11703072).

References

Burge, J., Davison, W., Martin, H., & Zhao, C. 2008, in Advanced Optical and Mechanical Technologies in Telescopes and Instrumentation, SPIE Conference Series, 7018, 701814

Burge, J. H., Kot, L. B., Martin, H. M., Zehnder, R., & Zhao, C. 2006, in Optomechanical Technologies for Astronomy, eds. E. Atad-Ettedgui, J. Antebi, & D. Lemke, 6273, International Society for Optics and Photonics (SPIE), 62730M

Chen, M., Cheng, W., & Wang, C.-W. W. 1992, in Laser Interferometry IV: Computer-Aided Interferometry, ed. R. J. Pryputniewicz, 1553, International Society for Optics and Photonics (SPIE), 626

Jiang, J., & Jiang, A. 2020, ASTRONOMICAL RESEARCH AND TECHNOLOGY, 17, 376 (in Chinese)

Li, S., Wu, F., Chen, Q., Fan, B., & Li, L. 2013, in Optical Measurement Systems for Industrial Inspection VIII, eds. P. H. Lehmann, W. Osten, & A. Albertazzi, 8788, International Society for Optics and Photonics (SPIE), 854

Lindlein, N. 2001, Appl. Opt., 40, 2698

Peng, J., Chen, Z., Zhang, X., Fu, T., & Ren, J. 2015, Appl. Opt., 54, 7433

Wyant, J. C., & Bennett, V. P. 1972, Appl. Opt., 11, 2833

Xun, H., Zhang, Z., Bai, X., et al. 2020, Imaging Science and Photochemistry, 38, 377 (in Chinese)

Zeng, X., Zhang, X., Xue, D., Zhang, Z., & Jiao, J. 2018, Appl. Opt., 57, F56

Zhao, C., & Burge, J. H. 2007, Opt. Express, 15, 18014

Zhao, C., & Burge, J. H. 2008, Opt. Express, 16, 6586

Zhao, C., & Burge, J. H. 2009, in Optical Manufacturing and Testing VIII, eds. J. H. Burge, O. W. Fhnle, & R. Williamson, 7426, International Society for Optics and Photonics (SPIE), 253

Zhou, P., & Burge, J. H. 2007, Opt. Express, 15, 15410